Full Text View

Volume 30, Issue 12 (December 2000)

Journal of Physical Oceanography
Article: pp. 3039–3049 | Abstract | PDF (457K)

Statistics of "Synoptic Circulation Weather" in the North Sea as Derived from a Multiannual OGCM Simulation

Frank Kauker and Hans von Storch

Institute of Hydrophysics, GKSS Research Centre, Geesthacht, Germany

(Manuscript received February 22, 1999, in final form January 14, 2000)

DOI: 10.1175/1520-0485(2000)030<3039:SOSCWI>2.0.CO;2

ABSTRACT

A 15-yr simulation of an ocean general circulation model, exposed to atmospheric forcing as provided by the ECMWF reanalysis 1979–93, is analyzed with respect to the statistics of the surface circulation of the North Sea on timescales of days to several weeks in winter.

The first two EOFs of surface circulation are found to represent the bulk of the variability (72%). They are broadly consistent with the limited observational record. The first EOF represents regimes with one gyre flushing the entire North Sea, either with clockwise orientation (15% of time) or with counterclockwise orientation (30% of time). These regimes are excited by northeasterly and, respectively, southwesterly wind. The second EOF is representative for two opposite regimes with two bipolar patterns in the northern and southern part of the North Sea (45% of time). For a certain range of both EOFs coefficients, the North Sea circulation ceases (10% of time).

The circulation of the North Sea in winter is highly variable; the regimes change frequently. Only 40% of the one-gyre regimes persist for longer than 5 days, and the bipolar pattern regimes rarely extend for more than 5 days.

1. Introduction

The North Sea as a dynamical system attracts our interest for various reasons. This interest is partly reflecting our scientific curiosity, and is partly due to the importance of the North Sea for various socioeconomic aspects, ranging from fisheries, the transport of matter, and more generally, water quality. For these purposes, we are in need of reliable information about the dynamical state of the North Sea; we need to know the range of natural variability in terms of phenomena, intensity, and temporal and spatial extension.

The dynamics of the oceans as well as the atmosphere is characterized by the presence of infinitely many processes operating on a wide range of spatial and temporal scales. Therefore, mapping the instantaneous state of the oceans, or the atmosphere, is far from trivial, and can hardly be done from observations alone. This task is particularly demanding for the oceans, where observations of the dynamical state—for instance, currents or stream function—require costly in situ operations. Because of this limitation, the international oceanographic community has embarked on the challenging undertaking of "operational oceanography," which by means of intelligent merging of dynamical understanding (i.e., quasi-realistic models), of educated guessing (i.e., routine forecasts), and routine in situ and remotely sensed observations of a wide range of variables allows for a instantaneous, synoptic analysis of the state of the ocean (Robinson et al. 1998). These endeavors are pursued under the umbrella of international projects such as GOOS and EUROGOOS.

Currently, multiyear time series of regularly prepared analyses of the state of the North Sea are available only for variables such as sea surface temperature (Becker and Pauly 1996) and coastal sea level at various tide stations. For circulation, such analyses are unavailable for an extented time period suitable for a statistical analysis of inter- and intradecadal variability. Instead, episodic data at selected vertical profiles and cross sections had to be relied upon (see, e.g., Furnes 1980 or Sündermann 1994). Numerical models have been applied to investigate the dependence of the circulation on the strength and direction of the wind (Backhaus 1993; Backhaus and Hainbucher 1987; Maier-Reimer 1975), but this kind of sensitivity studies does not give insights into the statistics of the circulation. Additionally, multiyear simulations (Langenberg et al. 1999; Flather et al. 1998; Smith et al. 1996; Pohlmann 1996) have been executed, which provide an educated guess of the temporal and spatial variability of the dynamical state. Unfortunately, these long-term integrations have not been analyzed with respect to the statistics of synoptic variability of the circulation. Also, they partially suffer from inhomogeneities in the atmospheric forcing fields.

We used a full-fledged ocean general circulation model—Oberhuber's (1993) isopycnical GCM—adapted to the particular situation of the North Sea and the neighboring shelf ocean [for details, refer to Kauker and Oberhuber (1997) and Kauker (1999)] forced with the homogeneous meteorological reanalysis provided by ECMWF (1979–93). The model, the forcing data, and the simulation are summarized in section 2. The skill of the model in reproducing observational evidence has been assessed by Kauker (1999); therefore, we limit ourselves to a few comparisons of simulated and "observed" data.

The simulated distributions of horizontal streamfunction at the surface was stored on a daily basis together with many other variables. In the present paper we analyze these data with the intention to identify and characterize circulation regimes (section 3). The analysis makes use of the standard multivariate technique of Empirical Orthogonal Functions or Principal Components (von Storch and Frankignoul 1998). The first two EOFs turn out to represent most of the large-scale variability of the North Sea circulation. This inspires the projection of the state of the North Sea onto the two-dimensional phase space spanned by the first two EOFs. Then, different parts of this 2D phase space are identified with different regimes. They are characterized by the circulation, the simultaneous air pressure fields, their residence time distributions, and probabilities for transfers between the regimes. Evidence from the observational record is compared with model results in section 4. In the concluding section 5 the results are related to hypotheses available from the literature, and a short general discussion of the value and limitation of using output from quasi-realistic ocean models as a substitute for observational data is offered.

2. OGCM, data

The regional Ocean isoPYCnic (OPYC) model (Kauker and Oberhuber 1997) is a derivative of Oberhuber's OPYC model, which has been found to be a flexible and reliable simulation tool by a variety of researchers (e.g., Miller et al. 1994; Holland et al. 1996; Lunkeit et al. 1996; Cabos Narvaez et al. 1998; Junge et al. 2000). In the present application, the model was adapted for describing variations of sea level, temperature, and salinity in the North Sea. Also the influence of the state of the adjacent oceans was to be studied. Therefore, the North Sea and the adjacent Northeast Atlantic as well as the Norwegian–Iceland–Greenland Seas (GIN Seas) is modeled. The model area is rotated and approximately given by the following four corners (37°4′N, 3°49′W), (44°44′N, 29°0′E), (61°49′N, 29°11′W), and (80°13′N, 25°44′W). The horizontal resolution varies from ½° × ½° at the lateral boundaries to 6′ × 6′ in the central North Sea. The topmost layer is formulated as a mixed layer. The deeper ocean is discretized in the vertical with 14 Lagrangian isopycnal layers. The three-dimensional OPYC model solves the primitive equation with a time step of 3 h, that is, solves the slow barotropic and baroclinic modes. A barotropic tide model, which solves the faster tidal modes, is coupled to the 3D model. The four strongest partial tides are prescribed at the lateral boundaries of the tide model. The 3D model is coupled to the tide model via the bottom stress and the residual circulation of the tide model.

The density varies according to advection of temperature and salinity as well as surface fluxes. An annual mean flux adjustment for heat and freshwater is applied in the Northeast Atlantic and the GIN Seas, but not for the North Sea. The freshwater input from the rivers is calculated with the help of a soil model and a discharge model.

The regional OPYC model is forced with surface data from the European Centre of Medium-Range Weather Forecasts (ECMWF) reanalysis project (Gibson et al. 1997). The data of the operational weather model of the ECMWF have the disadvantage that over time the weather model was continuously changed with respect to resolution and to parameterizations

of subgrid scale processes. Also, the initialization scheme was continuously updated. In 1993, the ECMWF decided to hindcast the time period 1979 to 1993 with a fixed setup, that is, with a fixed weather forecast model and a fixed data assimilation scheme. The selected weather model has a T106 horizontal resolution and 31 vertical layers. With the help of the data assimilation scheme, the *optimal* initial values are calculated. Here, the 12-hourly forecasts are used as forcing data for the regional OPYC model.

The advantage of the ECMWF reanalyses is their homogeneity: the weather model and the assimilation scheme are fixed and the output is dynamically consistent; that is, all variables are related via the underlying realizations of the physical processes of the weather model.

The heat and freshwater fluxes are calculated from the regional OPYC model in dependence of the 2-m air temperature, SST, dewpoint temperature, cloudiness, and precipitation. The solar radiation and the wind stress are taken from the reanalysis directly.

The skill of the model in reproducing "observed" features is demonstrated here by showing the winter-mean horizontal surface streamfunction (Fig. 1), and by comparing times series of sea level at Esbjerg (at the Danish coast of the North Sea, Fig. 2) and of the distribution of simulated and analyzed surface salinity concentrations in February 1982 (Fig. 3). For a more detailed validation of the model we refer to Kauker (1999).

The simulated winter (Dec, Jan, and Feb) mean circulation (Fig. 1) is organized in one counterclockwise gyre, flushing the entire North Sea in about 650 days with typical mean velocities of 10 cm s^{-1}. It compares well with estimates derived from observations (Svendsen et al. 1995).

The observed time series of sea level variations at Esbjerg are well reproduced by the model (Fig. 2) as is demonstrated by the similarity of the autospectra, a phase lag close to zero for all frequencies and the high squared coherency. Only for timescales shorter than, say, 2 days the power of the simulated auto spectrum falls off, and the coherency becomes notably smaller. This is not surprising as the model was constructed to simulate variations on timescales longer than several M_2 tides. As sketched above, the effect of the tides is included only in parameterized form.

The broad features of the surface salinity fields in February 1982 (ICES analysis; Fig. 3), like the minimum of less than 30 psu in the German Bight, the locations of the 34.5 and 35.1 psu isolines are simulated well. Features of smaller scale, such as the strong gradient between Denmark and Norway or the maximum in front of the Thames, are not captured. Since we are dealing only with large-scale features in the following analysis, the skill of the simulation may be considered satisfactorily.

3. Statistics of surface circulation regimes

From the daily horizontal fields of surface velocity streamfunction $\Psi(x, t)$ the covariance matrix has been determined and the eigenvalues λ_k and eigenvectors calculated. Before doing so, the data are centered; that is, the long-term mean distribution $\Psi(x)$ (Fig. 1) is subtracted. Thus, the analyzed fields are *anomalies* $\Psi'(x, t)$. The eigenvectors are the EOFs $\mathbf{E}_k(x)$. Their relative importance is measured by the eigenvalues, which equals the expected proportion of variance accounted for by the EOFs. That is, if the streamfunction field is expanded into EOFs with time coefficients $\psi_k(t)$

$$\Psi'(x, t) = \sum_k \psi_k(t)\mathbf{E}_k(x), \qquad (1)$$

then

$$\lambda_k = \mathrm{var}(\Psi) - \mathrm{var}(\Psi - \psi_k\mathbf{E}_k), \qquad (2)$$

where k counts the EOFs and var(·) represents a variance; note that var(Ψ) = var(Ψ'). In Eq. (2) and the following the dependence on x and t is omitted. The EOFs $\mathbf{E}_k$ are normalized so that their coefficient ψ_k have a standard deviation of 1. In technical terms $\langle \mathbf{E}_k, \mathbf{E}_k \rangle = \lambda_k$, with $\langle \cdot\,, \cdot \rangle$ representing the conventional dot product, and var(Ψ_k) = 1. Thus, the magnitude of the patterns may be considered "typical." Note that the sign of the EOFs is undetermined, as is always with EOFs. [For a detailed introduction of EOFs and related statistical analysis techniques, refer to von Storch and Frankignoul (1998) or von Storch and Zwiers (1999)].

The first eigenvalue is λ_1 = 52% × var(Ψ), that is, the first EOF accounts for 52% of the 1979–93 winter variance. The

second describes 20% of the variance. Thus, considering only the first two EOFs in our statistical analysis means that only 28% of the variance is disregarded.

The first two EOFs $\mathbf{E}_k$, with $k = 1, 2$, together with their time coefficients ψ_k are displayed in Fig. 4. The first EOF features one gyre covering the entire North Sea, with a clockwise or counterclockwise orientation depending on the sign of the coefficient. In the second EOF, two smaller gyres of opposite orientation are located in the southern and northern part of the North Sea. Consistently with the difference in eigenvalues, the magnitude of $\mathbf{E}_2$ is considerably smaller than that of $\mathbf{E}_1$.

The time coefficients vary irregularly, exhibiting some variability on time scales of weeks. While EOF 2 is short lived, the coefficient ψ_1 of the first EOF $\mathbf{E}_1$ exhibits extended persistent episodes, as for instance a prolonged period of clockwise circulation ($\psi_1 > 0$) in February 1986 [the value of the coefficient is close to 2 (standard deviations) for almost the whole month in the middle of the time series].

All daily states ($\psi_1(t)$, $\psi_2(t)$) are displayed as a scatter in Fig. 5. The points are regularly distributed similar to two independent standard Gaussian distribution (which is not surprising in view of the normalization and that the EOF coefficients are constructed to be independent), even though there is an indication that the distribution of ψ_1 (along the horizontal axis) may be a bit skewed to the right. A visual inspection of Fig. 5 reveals no further structure in the scatter; this finding is substantiated by a cluster analysis that returned no meaningful partitioning of the scatter.

The EOF coefficient time series ψ_k are used to define the regimes. For that purpose, first that pair of coefficients (ψ^*_1, ψ^*_2) is determined such that the reconstruction $\psi^*_1\mathbf{E}_1 + \psi^*_2\mathbf{E}_2$ represents a state with almost no circulation. The "no circulation" point (ψ^*_1, ψ^*_2) is found by minimizing the area-averaged standard deviation of $\Psi - \psi_1\mathbf{E}_1 - \psi_2\mathbf{E}_2$. This condition is fulfilled by $\psi^*_1 = 0.4$ and $\psi^*_2 = -0.3$. The states in the neighborhood, given by a circle containing 10% of all states, are considered "weak circulation" and collected into class V.

The patterns of the EOFs indicate that we may expect for negative ψ_1 an intensification of the time mean counterclockwise circulation, for large positive ψ_1 a reversal, and that relatively small ψ_1 will be associated with smaller scaled configurations, dependent on the sign of ψ_2. To characterize these four possible configurations, we partition the 2D (ψ_1, ψ_2) plane into four sectors, labeled I, II, III, and IV, while leaving out the circle labeled V around the "no circulation" point (ψ^*_1, ψ^*_2). The four sectors as well as the circle are given in Fig. 5. Fifteen percent of all cases belong to sector I, 30% to sector II, 30% to sector III, and 15% to sector IV. These numbers are to some extent arbitrary, as the size of the circle V was chosen to contain 10% of all cases.

For each of the four sectors $\mathbf{X}$ = I, II, III, and IV as well as for the circle V, mean circulations are calculated. These mean circulations are the composites

$$\overline{\Psi}_X = \frac{1}{|X|} \sum_{(\psi_1,\psi_2)\in X} \Psi, \qquad (3)$$

where $|X|$ is the number of elements in $\mathbf{X}$. Note that the composites are not calculated from anomalies Ψ' but from the full fields Ψ. The resulting five distributions are displayed in Fig. 6.

As expected, the composite for sector I, Ψ_{I}, exhibit a clockwise circulation, opposite to the time mean circulation, sector II a bipolar circulation (Ψ_{II}) with a counterclockwise circulation in the northern part, sector III an intensified counterclockwise circulation (Ψ_{III}), sector IV a kind of dipole with a counterclockwise circulation in the southern part (Ψ_{IV}), and circle V no significant structure (Ψ_{V}).

In the same manner, composites $\overline{p}_X$ of surface air pressure have been calculated and are displayed in Fig. 7. According to these maps, a reversed circulation takes place when northeasterly winds prevail (compare Ψ_{I} with $\overline{p}_{\mathrm{I}}$), and an intensified circulation when the wind is southwesterly. The smaller counterclockwise gyre in the northern part is connected

with southwesterly wind, and the counterclockwise gyre in the southern part with northerly winds. Weak westerly winds prevail when the circulation is weak.

The EOF coefficients (ψ_1, ψ_2) represent a kind of index, which allows one to classify each day as belonging to one of our five categories, I to V. This index allows us to calculate distributions of *residence times*, that is, frequencies of occurrence that the system remains in a given regime for at least n consectutive days. In Fig. 8 these are normalized so that the probability for remaining at least $n = 1$ day in a given regime is set to 1. (Of course, the probability for entering a certain regime is not uniform, as described above.)

According to Fig. 8 the regimes I and III, with an intensified or reversed basinwide circulation, are considerably more persistent than regimes II and IV as well as V. Forty percent of initial intensified, or reversed, circulations will persist for 5 or more days, whereas regime II will persist only in 15% and regime IV only in less than 10% of the time for 5 or more days. A situation with almost no circulation will also persist only for a short time.

We speculate that the different persistence of the regimes is related to the persistence of the forcing fields (a blocking situation in regime I, for instance), and not due to some internal dynamical reasons.

With the help of the index, we may also quantify the likelihood of changes from one regime to any other. The absolute frequency of changes is listed in Table 1. Obviously, the most frequent event is "no change," but *when* a change takes place, then there is a clear preference of a sequence I $\rightarrow$ II $\rightarrow$ III $\rightarrow$ IV $\rightarrow$ V, with a return to I most often via IV and V. When comparing these sequences with the air pressure, composites in Fig. 7 appear to be associated with the passage of a low pressure system in easterly direction across the North Sea.

4. Consistency with the observed sea level record

The question arises whether the two modes found in the multiyear simulation are consistent with the observational record. As mentioned in the introduction, a direct comparison with "observed" circulation data is impossible for the time being since multiyear analyses of circulation are unavailable. Furthermore the comparison with data from spatially and temporarily limited observational campaigns is inconclusive. For instance, the Furnes (1980) analysis of data collected during JONSDAP 1976 covers only 2 months of observations on a cross section between Scotland and Norway. All that can be said is that our first mode is consistent with his findings. But what about the second mode?

The only extended, homogeneous dataset available is sea level recorded at a number of tide gauges along the coast. We had the data from Wick, Aberdeen (UK), Hoek van Holland, Den Helder, Delfzijl (NL), Cuxhaven (D), Esbjerg (DK), and Smogen (S) at our disposal.

We regressed the coefficients ψ_1 and ψ_2 of the first two circulation EOFs (Fig. 4) on the sea level variations $z_j(t)$ at the $j = 1, \ldots, 8$ gauges along the North Sea coast; that is, we determined numbers $\gamma_{i,j}$ such that

$$\sum_t (\psi_i(t) - \gamma_{i,j} z_j(t))^2 = \min. \qquad (4)$$

We used both observed and simulated sea level variations. The resulting numbers $\gamma_{i,j}$ are displayed as curves in Fig. 9. Keeping in mind that the tide gauges reflect to some extent local effects unknown to the dynamical model, the similarity between the regression coefficients for the observed and simulated sea level variations is remarkable for both EOFs.

The projection of the first EOF (Fig. 4) on the coastal sea level reveals a general lowering of the water level, of the order of 20 to 40 cm. This lowering is consistent with the anomalous counterclockwise circulation, with strongest gradients off the Danish coast (i.e., Esbjerg) and weakest gradients along the Scottish coast (Wick, Aberdeen). The argument is linear so that a negative EOF coefficient $\psi_1(t)$ is associated with higher sea levels along the coasts.

The second EOF (Fig. 4) is composed of smaller-scaled features; these are reflected in the regression coefficients. The minima in streamfunction, located off the Scottish and the Danish coast, represent clockwise circulations and are consistently associated with an increase of coastal sea level (of the order of 10 cm), whereas in the southern North Sea an anomalous counterclockwise circulation prevails. Consistently, the sea level anomalies are negative along the Dutch and German coast.

That the OGCM generates a dynamically consistent link between the circulation patterns and coastal sea level variations is not surprising, as the model has been constructed to be dynamically consistent. However, that similar patterns emerge from

the observational record is not trivial; indeed, this is a strong support for the reality of both EOF patterns.

5. Conclusions

The results of the present study may be summarized as follows.

1. The statistics of large-scale surface circulation of the North Sea is a two-dimensional phenomenon and may be described by the first two EOFs. Both EOFs are found compatible with the observational record.

2. With the help of the first two EOFs a set of four regimes may be defined, which differ in their dynamical characteristics. The regimes change frequently, only about 20% of a regime persists for more than 5 days. That is, the North Sea circulation is highly variable with characteristic times of a few days.

3. Two regimes, associated with EOF 1 of the surface velocity streamfunction, exhibit one basinwide gyre, with an intensified time mean circulation or a reversed time mean circulation. The former is linked to southwesterly winds and prevails about one-third of the time, whereas the latter is linked to northeasterly winds and appears 15% of the time. Both regimes persist 40% of the time for 5 days or longer.

4. Two other regimes, associated with EOF 2, exhibit a bipolar pattern with opposite gyres in the northern and southern part of the North Sea. These structures are connected with southerly and northerly winds and are short lived. The southerly wind regime persists for 5 or more days 20% of the time, whereas the northerly wind regime persists for 5 or more days only 5% of the time.

5. The regimes often undergo a sequence, which is characteristic for the passage of a low pressure system across the North Sea.

The results are qualitatively in accord with the hypotheses of Furnes (1980) and Backhaus (1993), even if certain aspects, such as the characteristic wind directions associated with the different “circulation regimes,” deviate somewhat from Backhaus’ hypothesis.

The present analysis is meant to describe the statistics of the large-scale circulation in the North Sea. It is not meant to isolate extreme events, which by definition are rare events. Thus, it is not surprising that previous classifications of situations, related to heavy storm surges in the German Bight (Dolata et al. 1983) are not reflected in the present analysis.

The paper relies exclusively on model output, and no simple dynamical explanation has been offered for the appearance of the modes. How can we be sure, that we have learned something about the ocean? In fact, even if we have demonstrated the model’s ability to reproduce various observed features, we cannot exclude the possibility that some of our results stem from model artifacts (cf. Oreskes et al. 1994).

We claim, however, that the “substitute reality” of an OGCM allows formulation of hypotheses; these hypotheses must be verified with the observational record;at the present time this is possible only to a very limited extend as routine operational analyses run over a sufficiently long time are not yet available. We have compared our results with this limited observational evidence and found our results compatible.

It would of course be advantageous, if we could offer a “theoretical” argument for the emergence of our two modes. For the first mode, such arguments have been prepared by Furnes (1980), but for the second we are empty handed. Is it a “physical” mode? What is a “physical” mode? An eigenmode of a simplified dynamical equation, which may or may not have relevance for the system at hand? As discussed by von Storch and Frankignoul (1998), there is sometimes a strong correspondence between empirically derived modes and dynamical eigenmodes, but it happens as well that the necessary manipulations of the dynamical equations lead to oversimplifications so that statistical findings cannot be captured in this manner. This may be discouraging for theoretical oceanographers, but it is, unfortunately, sometimes the case with open, stochastically forced, multidimensional environmental systems.

We expect that future achievements will help clarifying the remaining problems. These achievements will come by combining new observational data, improved modeling tools, and theoretical understanding (Navarra 1995). A more reliable database will be available after the successful implementation of operational analysis tools, run routinely for monitoring purposes. When such techniques will eventually have matured, certainly reanalysis projects, comparable to the reanalysis of atmospheric variability prepared by ECMWF and used in our study as forcing fields, will be undertaken and the existence of the second mode can be confirmed or disproved.

Acknowledgments

We thank Josef Oberhuber for his ongoing and unfailingly support and Matthias Stölzel for his cluster analysis of our data. The work was done in the framework of the EU project “ESEL.”

REFERENCES

Backhaus, J. O., 1993: Das “Wetter” im Meer: Nord- und Ostsee. *Klimaänderung Küste A,* **1/5338,** 37–49.

— , and D. Hainbucher, 1987: A finite difference general circulation model for shelf seas and its application to low frequency variability on the north European Shelf. *Three-Dimensional Models of Marine and Estuarine Dynamics,* J. C. J. Nihoul and B. M. Jamart, Eds., Elsevier, 221–224.

Becker, G. A., and M. Pauly, 1996: Sea surface temperature changes in the North Sea and their causes. *J. Mar. Sci.,* **53,** 887–898.

Cabos Narvaez, W., M. J. Ortiz Beviá, and J. M. Oberhuber, 1998: The variability of the tropical Atlantic. *J. Geophys. Res.,* **103C,** 7475–7489.

Dolata, L. F., E. Roeckner, and H. Behr, 1983: Prognostic storm surge simulation with a combined meteorological/oceanographic model. *North Sea Dynamics,* J. Sündermann and W. Lenz, Eds., Springer-Verlag, 266–278.

Flather, R. A., J. A. Smith, J. D. Richards, C. Bell, and D. L. Blackman, 1998: Direct estimates of extreme storm surge elevations from a 40 year numerical model simulation and from observations. *Global Atmos. Ocean Syst.,* **6,** 165–176.

Furnes, G. K., 1980: Wind effects in the North Sea. *J. Phys. Oceanogr.,* **10,** 978–984. Find this article online

Gibson, J. K., P. Kallberg, S. Uppala, A. Nomura, E. Serrano, and A. Hernandez, 1997: ERA description. ECMWF Reanalysis Project Report 1: Project organization. Tech. Rep. ERA PRS1, European Centre for Medium-Range Weather Forecasts, Reading, United Kingdom, 72 pp.

Holland, D. M., L. A. Mysak, and J. M. Oberhuber, 1996: Simulation of the mixed-layer circulation of the Arctic Ocean. *J. Geophys. Res.,* **101C,** 1111–1128.

Junge, M. M., J.-S. von Storch, and J. M. Oberhuber, 2000: Large-scale variability of the main thermocline excited by stochastic wind stress forcing. *J. Climate,* **13,** 2833–2840. Find this article online

Kauker, F., 1999: Regionalization of climate model results for the North Sea. Ph.D. thesis, University of Hamburg, 109 pp. [Available as Tech. Rep. GKSS 99IEI6 from Library, GKSS Research Centre, P.O. Box 1160, D-21494 Geesthacht, Germany.].

— , and J. M. Oberhuber, 1997: An isopycnal ocean circulation model of the North Sea for dynamical downscaling. Tech. Rep. 97IEI47. [Available from Library, GKSS Research Centre, P.O. Box 1160, D-21494 Geesthacht, Germany.].

Langenberg, H., A. Pfizenmayer, H. von Storch, and J. Sündermann, 1999: Storm related sea level variations along the North Sea coast: Natural variability and anthropogenic change. *Contin. Shelf Res.,* **19,** 821–842.

Lunkeit, F., R. Sausen, and J. M. Oberhuber, 1996: Climate simulations with the global coupled atmosphere–ocean model ECHAM2/OPYC. Part I: Present-day climate and ENSO events. *Climate Dyn.,* **12,** 195–212.

Maier-Reimer, E., 1975: On the influence of a mean wind stress on the residual currents of the North Sea. *Dtsch. Hydrogr. Z.,* **28/6,** 253–262.

Miller, A. J., D. R. Cayan, T. P. Barnett, N. E. Graham, and J. M. Oberhuber, 1994: Interdecadal variability of the Pacific Ocean: Model response to observed heat flux and wind stress anomalies. *Climate Dyn.,* **9,** 287–302.

Navarra, A., 1995: The development of climate research. *Analysis of Climate Variability: Applications of Statistical Techniques,* H. von Storch and A. Navarra, Eds., Springer-Verlag, 3–10.

Oberhuber, J. M., 1993: Simulation of the Atlantic Circulation with a coupled sea ice–mixed layer–isopycnal general circulation model. Part I: Model description. *J. Phys. Oceanogr.,* **23,** 808–829. Find this article online

Oreskes, N., K. Shrader-Frechette, and K. Beltz, 1994: Verification, validation, and confirmation of numerical models in earth sciences. *Science,* **263,** 641–646.

Pohlmann, T., 1996: Predicting the thermocline in a circulation model of the North Sea. Part I: Model description, calibration and verification. *Contin. Shelf Res.,* **16,** 131–146.

Robinson, A. R., P. F. J. Lermusiaux, and N. Q. Sloan III, 1998: Data assimilation. *The Sea.* Vol. 10: *The Global Coastal Ocean: Processes and Methods,* K. H. Brink and A. R. Robinson, Eds., John Wiley & Sons, 541–593.

Smith, J. A., R. A. Flather, M. D. Smogen, P. E. Damm, and J. Patsch, 1996: An investigation into the variability of circulation and transport on the North-West European shelf using three hydrodynamic models. *Dtsch. Hydrogr. Z.*, **48,** 325–348.

Sündermann, J., 1994: The variable flow and transport fields in the North Sea. Results from the projects ZISCH and PRISMA. *Scientific Symposium on the North Sea Quality: Status Report 1993,* J. Anderson, H. Karup, and U. B. Nielson, Eds., Danish Environmental Protection Agency, 28–32.

Svendsen, E., A. Aglen, D. W. Iversen, D. W. Skagen, and O. Smedstadt, 1995: Influence of climate on recruitment and migration of fish stocks in the North Sea. *Climatic Change and Northern Fish Population.* A. Beamish, Ed., *Can. J. Fish. Aquat. Sci.,* **121,** 135–147.

von Storch, H., and C. Frankignoul, 1998: Empirical modal decomposition in coastal oceanography. *The Sea.* Vol. 10: *The Global Coastal Ocean: Processes and Methods,* K. H. Brink and A. R. Robinson, Eds., Wiley & Sons, 419–455.

— , and F. W. Zwiers, 1999: *Statistical Analysis in Climate Research.* Cambridge University Press, 494 pp.

Tables

Table 1. Frequency distribution for the dynamical state to move from state "*X*" within a day to "*Y*," abbreviated by $X \longrightarrow Y$

	Y					
X	$X \to$ I	$X \to$ II	$X \to$ III	$X \to$ IV	$X \to$ V	Sum
I $\to Y$	147	37	1	6	8	198
II $\to Y$	17	277	66	8	30	399
III $\to Y$	1	36	318	53	9	417
IV $\to Y$	20	11	23	116	34	204
V $\to Y$	14	37	9	21	50	131

Click on thumbnail for full-sized image.

Figures

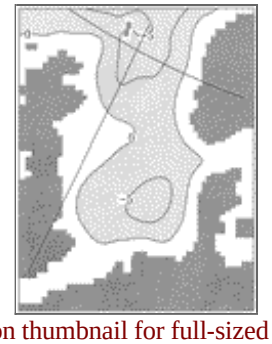

Click on thumbnail for full-sized image.

Fig. 1. Time mean horizontal surface velocity stream function Ψ in winter (Dec, Jan, and Feb). Negative values are shaded. The minimum describes a basinwide, counterclockwise circulation with an inflow in the west and an outflow in the east. The Greenwich meridian and the 60°N latitude line are shown to help with geographical orientation

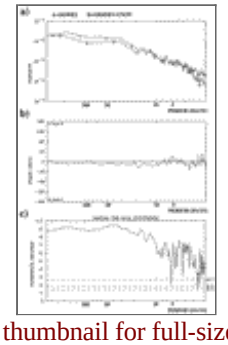

Click on thumbnail for full-sized image.

Fig. 2. Spectral analysis of simulated and observed sea level variations at Esbjerg (Denmark). (a) Autospectra: A represents the simulated data, B the observed data. (b) Phase spectrum: positive angles indicate that the simulated data lead the observed data, and negative angles that the observations lead the simulation. (c) Squared coherency spectrum: the dashed limits are thresholds,

allowing to reject the null hypothesis of zero coherency with a risk of 90%, 95%, and 99%

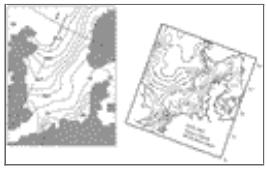

Click on thumbnail for full-sized image.

Fig. 3. Surface salinity distribution in Feb 1982 as analyzed by ICES (right; analysis from the “International Young Fish Survey 1982”) and simulated by the model (left)

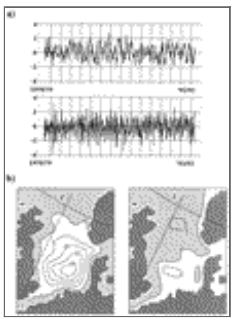

Click on thumbnail for full-sized image.

Fig. 4. The (a) EOF coefficients ψ_1 (top) and ψ_2 (bottom) are given for the winters 1979–93, beginning with Jan 1979 and ending with Dec 1993. The dashed vertical lines indicate the transition from one winter to the next. (b) First two EOFs $\mathbf{E}_1$ (left) and $\mathbf{E}_2$ (right) of daily surface velocity streamfunction simulated with the OPYC model forced with 1979–93 ECMWF reanalysis atmospheric fields. The EOFs are normalized so that the time coefficients have variance one [var(ψ_1) = var(ψ_2) = 1] and the patterns may be considered “typical” anomalies. Shading is used to discriminate between negative and positive values. Units: 10^3 m^2 s^{-1} for the patterns and none for the coefficients

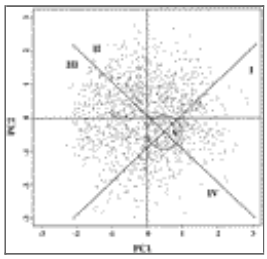

Click on thumbnail for full-sized image.

Fig. 5. Scatter diagram of the coefficients of the first two EOFs of North Sea surface velocity streamfunction. The horizontal axis represents the first coefficients and the vertical axis the second. The diagonal cross represents a partitioning of the 2D phase space, with the circle around the origin of this cross representing states with weak overall circulation. The four areas, labeled I, II, III, and IV, and the circle V, are discussed in the text. The time mean state corresponding to zero EOF coefficients is depicted in Fig. 1

Click on thumbnail for full-sized image.

Fig. 6. Composites Ψ_X of the surface velocity stream function Ψ, with X = I, II, III, IV, V as defined in Fig. 5. The panels are oriented as in Fig. 5, i.e., Ψ_{I} is on the right, Ψ_{II} on top, Ψ_{III} on the left, Ψ_{IV} at the bottom, and Ψ_{V} in the middle. Negative values are shaded. Units: 10^3 m^2 s^{-1}

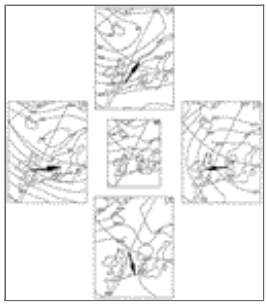

Click on thumbnail for full-sized image.

Fig. 7. Composites $\overline{p}_X$ of the air pressure p, with X = I, II, III, IV, V as defined in Fig. 5. The panels are oriented as in Figs. 5 and 6, i.e., $\overline{p}_{\mathrm{I}}$ is on the right, $\overline{p}_{\mathrm{II}}$ on top, $\overline{p}_{\mathrm{III}}$ on the left, $\overline{p}_{\mathrm{IV}}$ at the bottom, and $\overline{p}_{\mathrm{V}}$ in the middle. Units: hPa. The main direction of the wind stress is analyzed by composites of the wind stress (not shown) and sketched by an arrow

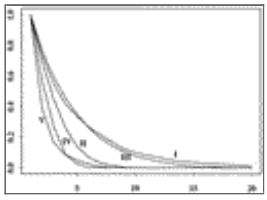

Click on thumbnail for full-sized image.

Fig. 8. Marginal probabilities for the circulations regimes to persist for at least n days, with n given on the horizontal axis

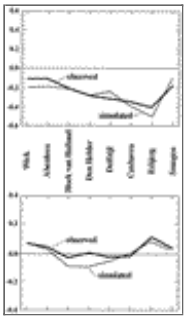

Click on thumbnail for full-sized image.

Fig. 9. Patterns of sea level variations at a number of coastal stations, derived by regressing the time coefficients of first two EOFs of simulated circulation. Heavy line: calculated from observed sea level; light line: calculated from simulated sea level. Units: m

Corresponding author address: Frank Kauker, Alfred-Wegener-Institute for Polar and Marine Research, P.O. Box 12 01 61, D-27515 Bremerhaven, Germany.

E-mail: fkauker@awi-bremerhaven.de

top